Available online at www.sciencedirect.com

ScienceDirect

IFAC Papers Online CONFERENCE PAPER ARCHIVE

IFAC-PapersOnLine 49-14 (2016) 001–006

Mechatronic Laboratory Setup For Study Of Controlled Nonlinear Vibrations ⋆

Boris Andrievsky *,*** **Vladimir I. Boikov** **
Alexander L. Fradkov *,**,*** **Ruslan E. Seifullaev** *,***

* *Institute for Problems in Mechanical Engineering of RAS, 61 Bolshoy prospekt, V.O., 199178, Saint Petersburg, Russia, boris.andrievsky@gmail.com, fradkov@mail.ru, ruslan.seifullaev@yandex.ru*
** *ITMO University, Saint Petersburg, Russia viboikov@mail.ru*
*** *Saint-Petersburg State University, 28 Universitetsky prospekt, 198504, Peterhof, Saint Petersburg, Russia*

Abstract: In the paper the results of first experimental studies with the setup are described, including motor parameters identification, state estimation and control of rotation velocity. The presented results demonstrate that the setup is useful for study and for control of complex nonlinear oscillatory systems.

Keywords: laboratory techniques, education, engineering, oscillation, nonlinear, control, estimation

1. INTRODUCTION

Mechatronics education requires an appropriate experimental facilities allowing instructors to implement modern project-based teaching and learning technologies. A number of educational laboratory setups for relatively simple and traditional units are described in the literature: for motors (Pogromsky and Van Den Berg, 2014), pendulum-like oscillators (Fradkov et al., 2014; La Hera et al., 2009; Oud et al., 2006), tanks (Pan et al., 2005; Starkov et al., 2012), etc. However there are only a few setups with multiple DOF systems allowing teachers to demonstrate complex nonlinear behavior and students to learn how to estimate and control it (Fradkov et al., 2012; Mayr et al., 2015).

This article describes a new teaching and research setup – the *Multiresonance Mechatronic Laboratory setup* (MMLS) and outlines its possible applications to control engineering education.

The rest of the paper is organized as follows. A brief description of the setup is presented in Sec. 2. Section 3 is devoted to modeling and parameter identification of the electric motor. The state estimation problem is addressed in Sec. 4. Section 5 presents some results on computer control of the vibrational stand, includi ng design of the PI-controller in the angular velocity loop and comparison of simulation and experimental results. Concluding remarks and an outline of possible applications of the setup are given in Sec. 6.

2. SETUP DESCRIPTION

The new device has been developed on the basis of many years of experience on creating vibrational stands at the Mekhanobr Engineering JSC and the IPME RAS (Blekhman, 2013; Tomchin and Fradkov, 2005). The MMLS includes the vibrational stand, electrical engines, sensors, and personal computer (PC). All the devices constitute an integrated system, where the electrical and mechanical processes are inextricably linked each other, which gives a basis to call the setup a *mechatronic* one. The mechanical part of the MMLS is an electrically driven vibrational device, see Fig. 1.

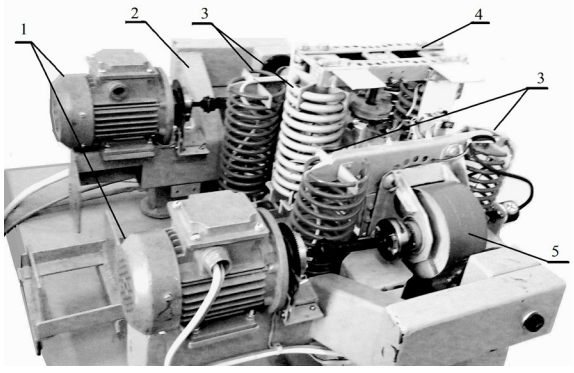

Fig. 1. Photo of the two-rotor vibrational stand. 1 – AC induction motors, 2 – support frame, 3 – springs, 4 – additional frame, 5– unbalanced rotor.

The key part of the stand is a pair of the unbalanced (centrifugal) actuators. Each actuator includes three-phase AC induction motor (1) with computer-controlled rotation velocity, the unbalanced rotor (5), which rotates on the motor shaft in a vertical plane on the stand carrier body.

⋆ The work was performed in the IPME RAS and supported by the Russian Science Foundation (grant 14-29-00142). The sample-data control system analysis (Sec.5.2) is supported by SPbSU (grant 6.38.230.2015)

10.1016/j.ifacol.2016.07.963

Unbalance of the rotor is provided by the eccentrically located weight. The drive shafts and the anti-vibration screw springs repeatedly reduce the stand table vibration transmission to the support frame (5) and to the basis, where the frame is located. The additional frame (4) is mounted on the stand table on the springs (3) for installing an additional weight.

The stand is equipped with five optical sensors measuring the table and the extra weight positions, velocity sensors with a resolution of 1000 pulses/revolution for two independently rotating rotors, as well as with the sensors of electric motor current. Set of the sensors can serve as a source of signals for studying and demonstrating the measuring systems, the signal processing, and the real-time control. For measuring positions of the stand table and the extra weight, the assemblies including eight linear and angular displacement sensors are installed. Each platform bears three angular and three linear optical encoders. Measured data from all the 12 sensors are transmitted to computer. The PC is supplied with the *ICP DAS* connector boards. 18 analog sensors are connected to the board for measuring the stand physical quantities. Four pulse sensors (encoders) *PISOEncoder600* of the shafts rotation angles of the stand are connected to the board.

Real-time data processing and control are carried out by means of Simulink Desktop Real-Time^{TM} of MATLAB© software. Control signal computation can be performed with a sampling rate up to 1000 Hz. In parallel, time histories of the chosen variables may be displayed on the PC monitor.

More detailed description of the MMLS may be found in (Andrievsky et al., 2016).

3. IDENTIFICATION OF THE ELECTRIC MOTOR PARAMETERS

3.1 Asynchronous motor model

The input of the frequency converter is fed by the dimensionless digital control signal u from the range of $[0, 65000]$, the measured output is angular velocity ω of the unbalanced rotor.

The initial part of the students' research includes the electric motor model parameter identification based on the experimental data, obtained from the setup. For the sake of simplicity, the following motor transfer function from control signal u to angular velocity ω (including the frequency converter, induction motor as such, and the unbalanced rotor) is taken:

$$W_d(s) = \left\{\frac{\omega}{u}\right\} = \frac{K_d}{(Ts+1)(\tau s+1)}, \qquad (1)$$

where K_d denotes the motor static gain; T and τ are time constants; $s \in \mathbb{C}$ denotes the Laplace transform variable. Since model (1) gives only a linear representation of the nonlinear AC motor dynamics for a certain operation area and does not describe the complex influence of revolving the unbalanced rotors and vibrating mechanical parts of the stand to the motor behavior, an essential part of the students' research is an experimental evaluation of the accepted assumptions for the real-world control and estimation problems. In what follows, the angular velocities in the range of $[80, 120]$ rad/s are picked up for the example.

3.2 Application of the optimization procedure

Firstly, consider minimization of the mean-square error between actual $\omega(t)$ and simulated ω_{sim} outputs for the same control input signal $u(t)$. The cost function is chosen in a form $J = \dfrac{1}{T_f - t_0}\int\limits_{t_0}^{T_f} e^2(t)\,dt$, where $e(t) = \omega(t) - \omega_{\text{sim}}(t)$, t_0, T_f are, respectively, the initial and the final instants for error evaluating. Signals $u(t)$, $\omega(t)$ are recorded during the experiment, $\omega_{\text{sim}}(t)$ is calculated by means of Simulink toolbox with zero initial conditions and $u(t)$ as an input signal. The value of $J = J(T, \tau, K_d)$ is used as an optimization cost for direct search Nelder-Mead MATLAB routine *fminsearch*.

Results of the identification procedure are illustrated by Fig. 2, where the time histories for initial ("guessed") parameter values $\hat{K}_d = 0.006$, $\hat{T} = 2$ s, $\hat{\tau} = 0.1$ s) and the optimized ones ($\hat{K}_d = 0.004$, $\hat{T} = 1.34$ s, $\hat{\tau} = 0.22$ s) are plotted. For the "right" motor this procedure leads

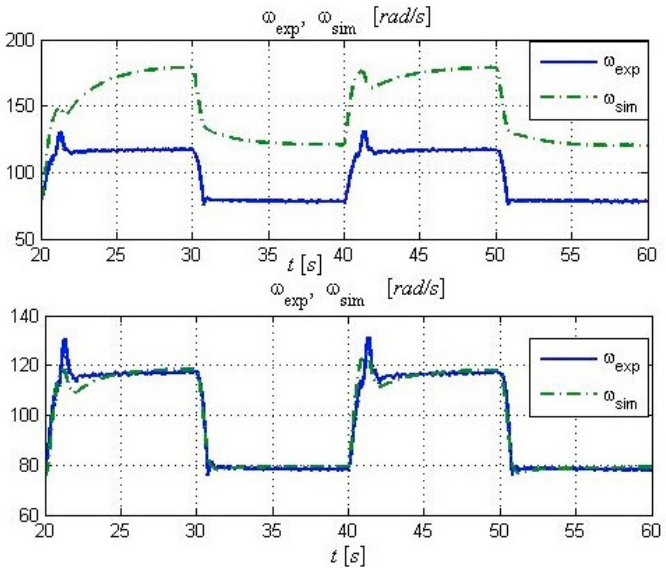

Fig. 2. Transients for initial (upper plot) and optimized (lower plot) parameters of the "left" motor.

to $K_d = 0.0040$ rad/s, $T = 1.28$ s, $\tau = 0.25$ s.

3.3 Application of non-recursive LSE method

Secondly, let us apply the least-square estimation (LSE) method. To this end, model (1) is expressed as the *linear regression* equation:

$$y[k] = \varphi[k]^{\mathrm{T}}\theta + v[k], \qquad (2)$$

where $y \in \mathbb{R}^1$ denotes the plant output at step $k = 1, 2, \ldots, N$, vector $\varphi[k] \in \mathbb{R}^m$ is the *regressor*, $\theta \in \mathbb{R}^m$ is the vector of plant model parameters, subjected to identification, m is a number of plant parameters, $v[k]$ is an additional noise (see (Ljung, 1999) for details).

The non-recursive LSE procedure leads to the following estimate of θ: $\hat{\theta} = \Phi^{\dagger}Y$,

where $\Phi = \begin{bmatrix} \varphi_1[1] & \dots & \varphi_m[1] \\ \vdots & & \vdots \\ \varphi_1[N] & \dots & \varphi_m[N] \end{bmatrix}$, $Y = \begin{bmatrix} y[1] \\ \vdots \\ y[N] \end{bmatrix}$.

For the considered case, model (1) may be represented as

$$\omega(t) = -\theta_1\ddot{\omega}(t) - \theta_2\dot{\omega}(t) + \theta_3 u(t), \qquad (3)$$

where $\theta_1 = T\cdot\tau$, $\theta_2 = T+\tau$, $\theta_3 = K_d$. To avoid using the time derivatives of $\omega(t)$, two 3rd order low-pass *state filters* are introduced as $W_f(s) = \dfrac{\mu}{s^3+3\mu s^2+3\mu^2 s+\mu^3}$, where $\mu > 0$ stands for the filter bandwidth. Measured signals $\omega(t)$, $u(t)$ are passed to the inputs of the corresponding filters. Finally, for (2) one obtains: $y[k] = \omega_f(t_k)$, $\varphi_1[k] = \ddot{\omega}_f(t_k)$, $\varphi_2[k] = \dot{\omega}_f(t_k)$, $\varphi_3[k] = \ddot{\omega}_f(t_k)$, where $t_k + t_0 = kT_0$, $k = 1,2,\dots,N$, T_0 is a chosen sampling interval, initial time t_0 is introduced for avoiding transient influence on the estimation results. Estimates $\hat{K}_d[k]$, $\hat{T}[k]$, $\hat{\tau}[k]$ of the motor parameters K_d, T, τ are calculated based on $\hat{\theta}[k]$ as follows: $\hat{\tau}[k]\cdot\hat{T}[k] = \hat{\theta}_1[k]$, $\hat{\tau}[k]+\hat{T}[k] = \hat{\theta}_2[k]$, $\hat{K}_d[k] = \hat{\theta}_3[k]$.

In the present study $t_0 = 10$ s, $T_0 = 0.05$ s, $\mu = 5$ s^{-1}, $N = 800$ are picked up. Application of the LSE procedure to the "left" motor gives $\theta = [0.3482, 1.556, 0.0039]^{\mathrm{T}}$, $\hat{K}_d = 0.0039$ rad/s, $\hat{T} = 1.285$ s, $\hat{\tau} = 0.271$ s.

3.4 Application of the recursive identification procedure

Thirdly, consider the following *recursive LSE* algorithm:

$$\begin{aligned} &\delta[k] = y[k] - \varphi[k]^{\mathrm{T}}\hat{\theta}[k-1], \\ &\Gamma[k] = \frac{P[k-1]\varphi[k]}{1+\varphi[k]^{\mathrm{T}}P[k-1]\varphi[k]}, \\ &P[k] = P[k-1] - \frac{P[k-1]\varphi[k]\varphi[k]^{\mathrm{T}}P[k-1]}{1+\varphi[k]^{\mathrm{T}}P[k-1]\varphi[k]}, \\ &\hat{\theta}[k] = \hat{\theta}[k-1] + \Gamma[k]\delta[k]. \end{aligned} \qquad (4)$$

with chosen $P[0] = P_0$, $P_0 = P_0^{\mathrm{T}} > 0$, $\hat{\theta}[0] = \theta_0$. Notations for variables $y[k]$, $\varphi[k]$ are the same as in Sec. 3.3. The students may be suggested to examine an influence of the LSE estimation algorithm parameters to the identification results.

As an example, the results for $t_0 = 10$ s, $T_0 = 0.05$ s, $\mu = 5$ s^{-1}, $P_0 = 10^3\mathrm{I}_3$ are plotted in Fig. 3. The plots show that the estimated variables converge to the final values in approximately ten seconds, and these values are very close to those obtained by the direct search optimization algorithm of Sec. 3.2 and the non-recursive LSE algorithm of Sec. 3.3. One may notice that the estimation convergence period gets on one-two transients. The steady-state values of the parameter estimates are following: $\hat{K}_d = 0.0039$ rad/s, $\hat{T} = 1.2782$ s, $\hat{\tau} = 0.2726$ s.

4. STATE ESTIMATION

After identification of the plant model parameters, the state estimation observer may be designed and its properties be studied.

4.1 State estimation over the unlimited bandwidth communication channel

Let us design the observer of full order based on the pole-placement technique. To this end, represent motor model

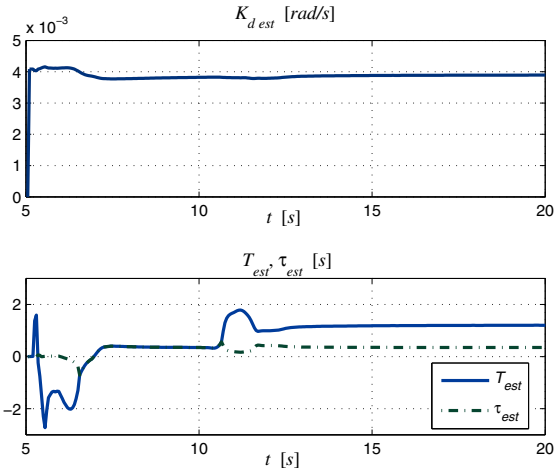

Fig. 3. Time histories of estimates $\hat{K}_d$, $\hat{T}$, $\hat{\tau}$ by means of the recursive LSE algorithm.

(1) in the following state-space form

$$\begin{aligned} &\dot{x}(t) = Ax(t) + Bu(t), \quad y(t) = Cx(t), \\ &A = \begin{bmatrix} 0 & 1 \\ -\dfrac{1}{T\cdot\tau} & -\dfrac{T+\tau}{T\cdot\tau} \end{bmatrix}, \quad B = \begin{bmatrix} 0 \\ \dfrac{K_d}{T\cdot\tau} \end{bmatrix}, \\ &C = [1\ 0]. \end{aligned} \qquad (5)$$

The full-order observer describes by the equation:

$$\dot{\tilde{x}}(t) = (A - LC)\tilde{x}(t) + Ly(t) + Bu(t), \qquad (6)$$

where $\tilde{x}(t)$ denotes the plant state $x(t)$ estimate, $L \in \mathbb{R}^{2\times 1}$ is the observer gain matrix (the design parameter). To find matrix L the pole-placement technique of the MATLAB routine *place* may be used. For the case of the Butterworth target polynomial $\det(s\mathrm{I} - LC) = s^2 + 1.4\Omega s + \Omega^2$, one obtains $L = [-2.47, 13.7]^{\mathrm{T}}$ as $\Omega = 2$ s^{-1} and $L = [8.73, 50.6]^{\mathrm{T}}$ as $\Omega = 10$ s^{-1}. The corresponding time histories of $\omega(t)$, $\tilde{\omega}(t)$ and angular acceleration $\varepsilon(t)$, $\tilde{\varepsilon}(t)$ are pictured in Figs. 4, 5.

The students should study dependencies of the estimation precision on parameter Ω, build the reduced-order Luenberger observer and apply the Kalman-Bucy filtering design technique. The estimation of the angular acceleration may be further used for PID-controller design.

4.2 State estimation under the data rate limitations

During the last decade substantial interest has been shown in networked control systems (NCS), which are real-time systems where sensor and actuator data are transmitted through shared or switched communication networks, see (Ishii and Francis, 2002; Nair et al., 2007; Matveev and Savkin, 2009). Studying the networked estimation and control problems is an essential part of modern control engineering education.

Let us demonsrate how the experimental data, obtained from the MMLS may used for studying the low-rate data transmission technology of (Fradkov et al., 2010).

Consider plant model (5). The problem is to produce the state estimation for (5) over the digital communication channel with the limited bandwidth. The coder of the *full order* embeds the observer. In (Fradkov et al., 2010),

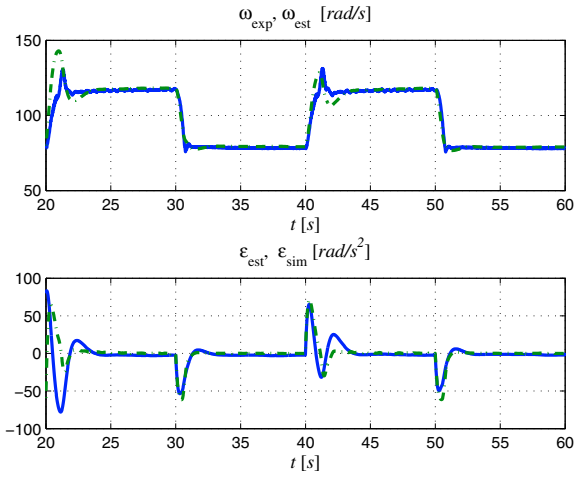

Fig. 4. Estimates of angular rate $\hat{\omega}(t)$ and angular acceleration $\hat{\varepsilon}(t)$ obtained by the observer for $\Omega = 2$ s^{-1} compared with the experimental $\omega(t)$ and simulation $\varepsilon(t)$ results.

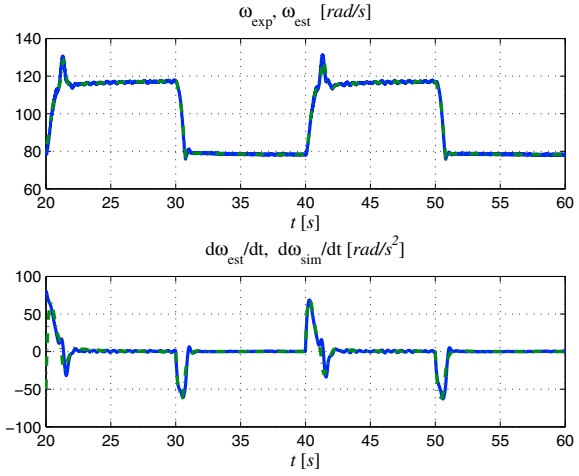

Fig. 5. Estimates of angular rate $\hat{\omega}(t)$ and angular acceleration $\hat{\varepsilon}(t)$ obtained by the observer for $\Omega = 10$ s^{-1} compared with the experimental $\omega(t)$ and simulation $\varepsilon(t)$ results.

the *observation error* (*innovation signal*) is transmitted over the channel rather than a measured plant output. For describing a such kind of the coders, let us introduce the error between the the plant and observer outputs as $\varepsilon(t) = y(t) - \hat{y}(t) = Ce(t)$. Error $\varepsilon(t)$ is sampled with a sampling rate T_0 and is represented in finite-length codeword by the following uniform binary quantizer:

$$q_\nu(y) = M\,\mathrm{sign}(\varepsilon), \tag{7}$$

where $M > 0$ is a real number (the *quantizer range*), $\mathrm{sign}(\cdot)$ is the signum function. Quantized signal $\bar{\varepsilon}[k] = M\,\mathrm{sign}\big(\varepsilon(t_k)\big)$, $t_k = kT_0$, $k = 0, 1, \ldots$ is transmitted over the channel at instants t_k. The following state estimation algorithm is implemented by the coder:

$$\begin{aligned} &\dot{\hat{x}}(t) = A\hat{x}(t) + Bu(t) + L\bar{\varepsilon}(t),\ \hat{y}(t) = C\hat{x}(t),\\ &\bar{\varepsilon}(t) = \bar{\varepsilon}[k] \ \text{ as } \ t \in [t_k, t_{k+1}),\ \ t_k = kT_0, \end{aligned} \tag{8}$$

where $\hat{x} \in \mathbb{R}^n$ stands for the estimate of plant state vector $x(t)$, cf. (6). The similar algorithm is reproduced by the decoder. Namely, signals $\bar{\varepsilon}[k]$ it the input of the decoder are expanded over the sampling interval $t \in [t_k, t_{k+1})$ producing stepwise signal $\bar{\varepsilon}(t) = \bar{\varepsilon}[k]$ which is applied to the observation algorithm

$$\dot{\tilde{x}}(t) = A\tilde{x}(t) + Bu(t) + L\bar{\varepsilon}(t),\ \hat{y}(t) = C\hat{x}(t), \tag{9}$$

where $\tilde{x}$ serves as a state estimate at the receiver's side; $\tilde{x}(0) = \hat{x}(0)$ should be taken.

The results of this data transmission and state estimation scheme for $T_0 = 0.05$ s, $M = 0.75$ are demonstarated in Fig. 6. Gain L is calculated for $\Omega = 20$ s^{-1}. The plots show that the maximal estimation error for the considered experimental data is less than 10 rad/s and mainly, $\varepsilon(t)$ is kept in the region ± 0.75 rad/s. Data transmission rate $R = T_0^{-1}$ in this experiment is as 20 bit/s. Increasing the data bitrate makes possible reducing the data transmission error.

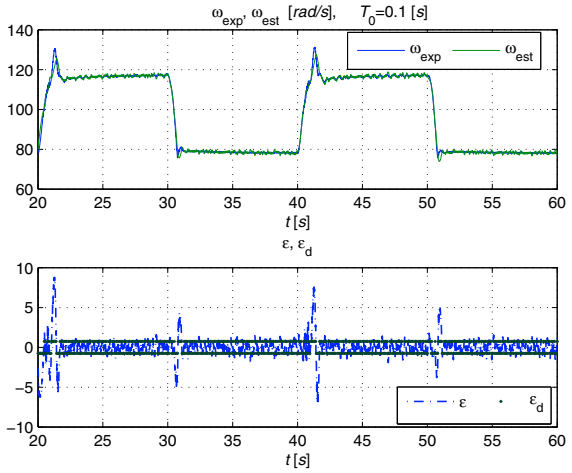

Fig. 6. Angular rate $\omega(t)$ and its estimate $\tilde{\omega}(t)$ over the digital binary communication channel with coder-decoder pair (7), (8), (9). $T_0 = 0.05$ s.

5. CONTROL OF ROTATION VELOCITY

5.1 Tuning the PI-controller to the magnitude optimum

To find the controller gains, approximate model (1) of the motor is taken. Let the proportional-integral (PI) control law be used for rotor velocity control. The PI-controller transfer function from tracking error to the control action has a form

$$W_c(s) = K_p + \frac{K_i}{s} = K_i\frac{T_c s + 1}{s}, \tag{10}$$

where K_p, K_i are the proportional and integral controller gains (respectively), and equivalent time constant T_c is introduced as $T_c = \dfrac{K_p}{K_i}$.

Following the magnitude optimum (MO) design method (Kessler, 1955; Toscano, 2005) for choice the PI-controller parameters, T_c is taken equal to T, which leads to compensation of dominant time constant T. Consequently, $K_p = TK_i$. Therefore, after equal pole and zero cancellation, the closed-loop system transfer function $\Phi(s)$ from

the reference (desired) rotation velocity ω^* to the actual one, ω, may be represented as

$$\Phi(s) = \left\{\frac{\omega}{\omega^*}\right\} = \frac{K_i K_d}{\tau s^2 + s + K_i K_d}. \quad (11)$$

For the considered system, the MO condition reads $(K_i K_d)^{-1} = 2\tau$, which leads to integral gain K_i as $K_i = \frac{1}{2\tau K_d}$. Taking into account the identification results of Sec. 3 for the left motor parameters, one obtains the PI-controller gains as $K_i = 400$ 1/rad, $K_p = 1040$ s/rad. In the learning process the students are also encouraged to use alternative design methods such as the frequency loop sharping, modal control, LQG optimization, etc.

5.2 Sample-data control system analysis

Consider system (1) and controller (10). Assume that the desired rotation velocity ω^* is a constant value. Open-loop system (1) can be rewritten in state-space form as follows:

$$\dot{\bar{x}}(t) = \bar{A}\bar{x}(t) + \bar{B}u(t), \quad \omega(t) = \bar{C}\bar{x}(t), \quad (12)$$

$$\bar{A} = \begin{bmatrix} -\frac{1}{T} - \frac{1}{\tau} & 1 \\ -\frac{1}{T\tau} & 0 \end{bmatrix}, \quad \bar{B} = \begin{bmatrix} 0 \\ \frac{K_d}{T\tau} \end{bmatrix}, \quad \bar{C} = [1\ 0].$$

Let $e(t) = \omega(t) - \omega^*$. Then one can write the state-space form of controller (10)

$$\dot{\nu}(t) = e(t), \quad u(t) = -K_p e(t) - K_i \nu(t). \quad (13)$$

Introduce the following notations:

$$r(t) = \bar{x}(t) - x^*, \quad x^* = \left[\omega^*, \frac{\omega^*}{T} + \frac{\omega^*}{\tau}\right]^T,$$
$$v(t) = u(t) - u^*, \quad u^* = \frac{\omega^*}{K_d},$$
$$\varepsilon(t) = \nu(t) - \nu^*, \quad \nu^* = \frac{-u^*}{K_d},$$
$$x(t) = \begin{bmatrix} r(t) \\ \varepsilon(t) \end{bmatrix}, \quad y(t) = \begin{bmatrix} e(t) \\ \varepsilon(t) \end{bmatrix}.$$

Then closed-loop system (12), (13) can be rewritten as follows:

$$\dot{x}(t) = Ax(t) + Bv(t), \quad y(t) = Cx(t), \quad (14)$$
$$v(t) = -Ky(t), \quad (15)$$

$$A = \begin{bmatrix} \bar{A} & \mathbf{0} \\ \bar{C} & 0 \end{bmatrix}, \quad B = \begin{bmatrix} \bar{B} \\ 0 \end{bmatrix}, \quad C = \begin{bmatrix} C & 0 \\ \mathbf{0} & 1 \end{bmatrix}, \quad K = \begin{bmatrix} K_p \\ K_i \end{bmatrix}.$$

Therefore, the goal $\omega(t) \xrightarrow[t\to\infty]{} \omega^*$ is equivalent to stabilization of (14).

Consider a sampled-time feedback control law

$$v(t) = -Ky(t_k), \ t_k \leqslant t < t_{k+1}, \quad (16)$$

where $\{t_k\}$ is an infinite sequence of sampling times $0 = t_0 < t_1 < \ldots < t_k < \ \ldots$, and $t_{k+1} - t_k \leqslant h$, for all $k \geqslant 0$ and some $h > 0$.

Closed-loop system (14), (16) is given by

$$\dot{x}(t) = Ax(t) - BKCx(t_k), \quad t \in [t_k, t_{k+1}]. \quad (17)$$

System (17) can be represented by the block diagram in Fig.7. Note that during the time between two sampling instants the feedback information is not updated, i.e. the system is in open-loop. Therefore, the sampling step h plays an important role for the system stability and has to be estimated.

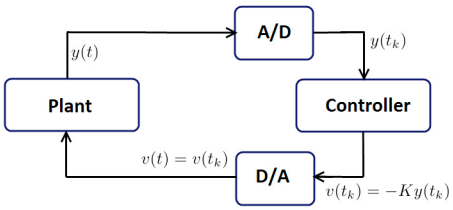

Fig. 7. Sampled-data system

Instead of the traditional reduction to discrete-time system (which loses information on the inter-sampling behavior) one can apply the method introduced by Emilia Fridman (Fridman's method, see e.g. (Fridman, 2014, 2010)). The approach consists in considering the effect of sampling as variable time-delay followed by the construction and use of a special Lyapunov-Krasovskii functional. As a result, the estimation of sampling step is reduced to feasibility analysis of linear matrix inequalities (LMI).

For the following parameter values: $K_d = 0.0045$ rad/s, $T = 1.35$ s, $\tau = 0.22$ s, $K_i = 400$ 1/rad, $K_p = 1040$ s/rad, $\omega^* = 110$ rad/s, the Fridman's method gives the maximum sampling period $h = 0.625$ (when system (17) is exponentially stable) that is about 96% from the simulation value.

Now assume that the control signal $v(t)$ of (16) passes through a block defined by

$$\Psi(v) = \begin{cases} v, & |v| \leqslant a, \\ \epsilon v + \operatorname{sign} v \cdot a(1-\epsilon), & |v| > a, \end{cases}$$

for some $a > 0, \epsilon \geqslant 0$. Note that for $\epsilon = 0$ it coincides with saturation. Then closed loop system (17) can be transformed as follows:

$$\dot{x}(t) = Ax(t) - B\varphi(KCx(t_k)) - BKC\varphi_0(KCx(t_k))x(t_k),$$

where

$$\varphi(v) = \begin{cases} 0, & |v| \leqslant a, \\ \operatorname{sign} v \cdot a(1-\epsilon), & |v| > a, \end{cases} \quad \varphi_0(v) = \begin{cases} 1, & |v| \leqslant a, \\ \epsilon, & |v| > a. \end{cases}$$

Since the function $\varphi(\cdot)$ is sector-bounded (with bounds 0 and $1-\epsilon$) and the function $\varphi_0(\cdot)$ is bounded for all t, one can use the extension of Fridman's method to a class of nonlinear system with sector-bounded nonlinearities proposed in (Seifullaev and Fradkov, 2016). The dependence of h on ϵ is shown in Fig. 8. Note that for $\epsilon = 1$ (i.e. $\Psi(\cdot) = id$) the maximum sampling period coincides with h, estimated by direct Fridman's method for linear systems.

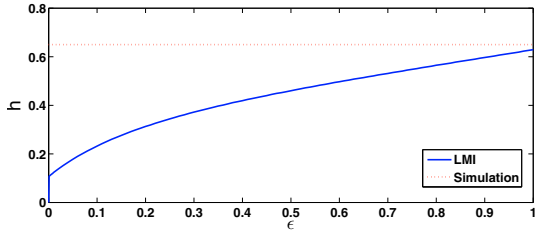

Fig. 8. The dependence of the maximum sampling period h on the parameter ϵ

5.3 Simulation and experimental results

Figure 9 demonstrates comparison of the experimental $\omega_{\text{exp}}(t)$, u_{exp} and the simulation $\omega_{\text{sim}}(t)$, u_{sim} results. The same square-waveform reference signal $\omega^*(t)$ has been applied to the real-world setup and the closed-loop system model with transfer function (11) and the parameter values, obtained via the identification procedure of Sec. 3.3. The results obtained shows a reasonable correspondence of the experimental and simulations data.

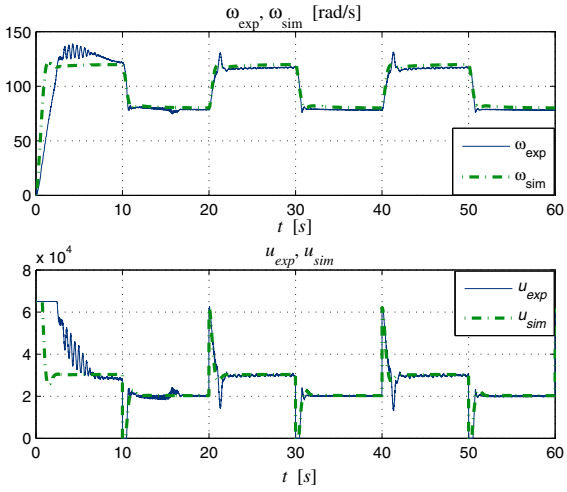

Fig. 9. Tracking the reference signal $\omega^*(t)$. Experimental $\omega_{\text{exp}}(t)$, $u_{\text{exp}}(t)$ and simulation $\omega_{\text{sim}}(t)$, u_{sim} results.

6. CONCLUSIONS

In the paper the results of first experimental studies with the novel research and educational mechatronic setup – the MMLS, created in the IPME RAS, including motor parameters identification, state estimation and control of rotation velocity are described. The MMLS makes it possible to study and demonstrate the various phenomena which arise in mechanical units, such as the phenomenon of self-synchronization, the Sommerfeld effect, start up of the unbalanced rotors rotation, the passage through the resonance area, the closed-loop control of the synchronization, etc. The presented results demonstrate that the setup is useful for study and for control of complex nonlinear oscillatory systems.

REFERENCES

Andrievsky, B., Blekhman, I.I., Blekhman, L.I., Boikov, V.I., Vasil'kov, V.B., and Fradkov, A.L. (2016). Education-research mechatronic setup for studying vibrational devises and processes. *J. Machinery Manufacture and Reliability.* To appear.

Blekhman, I.I. (2013). *Teoriya vibracionnyh processov i ustrojstv. Vibracionnaya mekhanika i vibracionnaya tekhnika (The theory of vibration processes and devices. Vibrational mechanics and vibrational engineering).* Publishing house "Ruda i metally", St. Petersburg. (in Russian).

Fradkov, A.L., Andrievsky, B., and Ananyevskiy, M.S. (2014). State estimation and synchronization of pendula systems over digital communication channels. *Eur. Phys. J. Special Topics*, 223, 773–793.

Fradkov, A.L., Andrievsky, B., and Peaucelle, D. (2010). Estimation and control under information constraints for LAAS helicopter benchmark. *IEEE Trans. Contr. Syst. Technol.*, 18(5), 1180–1187.

Fradkov, A.L., Andrievsky, B., and Boykov, K.B. (2012). Multipendulum mechatronic setup: Design and experiments. *Mechatronics*, 22(1), 76 – 82.

Fridman, E. (2010). A refined input delay approach to sampled-data control. *Automatica*, 46, 421–427.

Fridman, E. (2014). *Introduction to time-dalay systems.* Birkhäuser.

Ishii, H. and Francis, B.A. (2002). Stabilizing a linear system by switching control with dwell time. *IEEE Trans. Automat. Contr.*, 47(12), 1962–1973.

Kessler, C. (1955). Über die Vorausberechnung optimal abgestimmter Regelkreise. Teil III. Die optimale Einstellung des Reglers nach dem Betragsoptimum. *Regelungstechnik*, Jahrg, 3, 40–49.

La Hera, P.X., Freidovich, L.B., Shiriaev, A.S., and Mettin, U. (2009). New approach for swinging up the Furuta pendulum: Theory and experiments. *Mechatronics*, 19(8), 1240–1250.

Ljung, L. (1999). *System Identification: Theory for the User.* Prentice Hall, Upper Saddle River, NJ, USA. 2nd Ed.

Matveev, A.S. and Savkin, A.V. (2009). *Estimation and Control over Communication Networks.* Birkhäuser, Boston.

Mayr, J., Spanlang, F., and Gattringer, H. (2015). Mechatronic design of a self-balancing three-dimensional inertia wheel pendulum. *Mechatronics*, 30, 1–10.

Nair, G.N., Fagnani, F., Zampieri, S., and Evans, R. (2007). Feedback control under data rate constraints: an overview. *Proc. IEEE*, 95(1), 108–137.

Oud, W.T., Nijmeijer, H., and Pogromsky, A.Y. (2006). A study of Huijgens' synchronization: Experimental results. In K. Pettersen, J. Gravdahl, and H. Nijmeijer (eds.), *Group Coordination and Cooperative Control; Lecture Notes in Control and Information Sciences*, volume 336, 191–203. Springer, Berlin.

Pan, H., Wong, H., Kapila, V., and de Queiroz, M.S. (2005). Experimental validation of a nonlinear backstepping liquid level controller for a state coupled two tank system. *Control Engineering Practice*, 13, 27–40.

Pogromsky, A. and Van Den Berg, R. (2014). Frequency domain performance analysis of Lur'e systems. *IEEE Trans. Contr. Syst. Technol.*, 22(5), 1949–1955.

Seifullaev, R. and Fradkov, A. (2016). Robust nonlinear sampled-data system analysis based on Fridman's method and S-procedure. *International Journal of Robust and Nonlinear Control*, 26, 201–217.

Starkov, K.K., Kamp, H., Pogromsky, A.Y., and Adan, I. (2012). Design and implementation of a water-based emulator of manufacturing processes. In P. Pakshin (ed.), *Proc. 9th IFAC Symposium Advances in Control Education*, 396–410. IFAC, Nizhny Novgorod, Russia.

Tomchin, D.A. and Fradkov, A.L. (2005). Controlling passage of a rotor through the resonance band by the velocity-gradient method. *J. Machinery Manufacture and Reliability*, 5, 55–60.

Toscano, R. (2005). A simple robust PI/PID controller design via numerical optimization approach. *J. Process Control*, 15(1), 81–88.